Disrupted cholinergic modulation can underlie abnormal gamma rhythms in the schizophrenia

Jung Hoon Lee

Abstract

Gamma band oscillatory neural activity, considered critical in synchronizing brain areas, appears abnormal in patients with schizophrenia. Stimulus evoked gamma band power is lower, compared with healthy subjects, but baseline gamma power is higher. Based on the observation that cholinergic modulation regulates interactions between primary auditory cortex (A1) and an association cortex in the gamma frequency bands, we hypothesize that disrupted cholinergic modulation may underlie abnormal gamma rhythms in schizophrenia. In this study we use a computational model composed with pyramidal cells, fast-spiking (FS) and non-FS inhibitory interneurons. In accordance with experimental data, we simulate the pathological condition by lowering the excitability of non-FS cells. The spectral power densities of local field potentials (LFPs) are compared between control and pathological conditions in pre-stimulus and stimulus periods, respectively. In the simulations, disrupted cholinergic modulation enhances gamma band power in the pre-stimulus period but reduces it in the stimulus period, which is consistent with the patterns of experimentally observed abnormal gamma rhythms. We further note that top-down gamma rhythms suppress A1 responses and that A1 Pyr cells respond to top-down gamma rhythms in the pathological condition. Thus, we propose that cholinergic modulation can underlie the functional dysconnectivity and that the erroneous activation of A1 induced by top-down gamma rhythms in the pathological condition can account for auditory hallucination.

Introduction

Dysconnectivity hypothesis proposes that disturbed interactions among brain areas underlie the pathophysiology of schizophrenia (Pettersson-Yeo, Allen, Benetti, McGuire, & Mechelli, 2011; P. J. Uhlhaas, 2013), and recent studies have found disparate functional connectivity between healthy and schizophrenic subjects (Damaraju et al., 2014; Goñi et al., 2014; van den Heuvel & Hulshoff Pol, 2010). Notably, synchronous oscillatory activity in the gamma frequency band (alternative gamma rhythms) has been proposed to synchronize brain areas (Fries, 2005) and hence contribute to functional interactions among them. Together, one may expect the neural substrates of gamma rhythms to be aberrant in schizophrenia patients.

A line of studies has indeed reported abnormal gamma rhythms in schizophrenia patients (Pittman-Polletta, Kocsis, Vijayan, Whittington, & Kopell, 2015; P. Uhlhaas & Singer, 2010). For instance, the gamma band power in electroencephalography (EEG) induced by 40 Hz auditory click trains is lower in schizophrenia (Kwon et al., 1999; Vierling-Claassen, Cardin, Moore, & Jones, 2010). Interestingly, abnormal gamma rhythms appear to be independent from sensory stimuli. Spencer (Spencer, 2011) found that the baseline gamma power in the pre-stimulus period is higher, not lower in schizophrenia. This study seems consistent with the enhanced connectivity in the resting state networks (Andreou et al., 2015) and the higher absolute gamma synchrony (Flynn et al., 2008). As experimental and computational studies identify the neural circuits that generate gamma rhythms, one could infer schizophrenia's pathophysiology from abnormal gamma rhythms. It should be noted that the earlier computational models (Lee, Whittington, & Kopell, 2015; Spencer, 2009; Vierling-Claassen, Siekmeier, Stufflebeam, & Kopell, 2008) have already studied potential mechanisms behind the reduction of stimulus-evoked gamma rhythms, which has led to a few

theories, but the mechanisms behind the enhanced baseline gamma rhythms remain largely unknown.

This study investigates the potential pathophysiology of the enhanced baseline gamma rhythms in patients with schizophrenia. Recently, top-down gamma rhythms from higher order cognitive areas to lower order sensory cortices were reported in vision (Gregoriou, Gottes, Zhou, & Desimone, 2008) and auditory (Roopun et al., 2010) systems. This raises the possibility that endogenous signals induce baseline gamma rhythms. Then, what mechanisms could change the baseline gamma rhythms reflecting the endogenous signals? Our previous model study (Lee et al., 2015) proposed the necessity of cholinergic modulation in regulating coordination between top-down and bottom-up gamma rhythms merging in the superficial layer of primary auditory cortex (A1). Thus, we hypothesize that the disrupted cholinergic modulation underlies enhanced baseline gamma rhythms.

We address this hypothesis by building the superficial layer of A1 with three cell types (pyramidal (Pyr) cells, fast-spiking (FS) and non-FS inhibitory interneurons) and simulated the disruption of cholinergic modulation by lowering the excitability of non-FS cells which are known to have cholinergic receptors (Couey et al., 2007b; Gulledge, Park, Kawaguchi, & Stuart, 2007; Roopun et al., 2010; Xiang, Huguenard, & Prince, 1998). The simulation results support our hypothesis. In the pathological condition, in which non-FS cells become quiescent, we observed higher gamma rhythms in the pre-stimulus period (Spencer, 2011). Furthermore, in the pathological condition, top-down gamma rhythms in the model entrain A1 Pyr cells and induce A1 to send out erroneous sensory signals, suggesting that disrupted cholinergic modulation can cause auditory hallucination. We also observed that stimulus-evoked gamma rhythms are lower in the pathological condition,

which is consistent with experimental data (Kwon et al., 1999; Spencer, 2011; Vierling-Claassen et al., 2008) and our earlier model study (Lee et al., 2015).

Methods

We used the peer reviewed simulator named NEST (Gewaltig & Diesmann, 2007) to build the network model. All neuron models and synapse models are natively supported by NEST. As shown in Figure 1A, we implemented superficial layers of A1 and three external populations. Specifically, A1 consisting of 400 Pyr, 70 FS and 30 non-FS cells interacts with the three external populations of 100 Pyr cells (ovals in Figure 1A). First, HC mimics the higher order cognitive areas and projects 45 Hz sinusoidal Poisson spike trains into A1, as unidirectional signals from an association cortex to A1 were found at ~45 Hz (Roopun et al., 2010). Second, SC mimics bottom-up thalamic inputs induced by 40 Hz auditory click trains and thus projects 40 Hz sinusoidal Poisson spike trains into A1. These sinusoidal Poisson spike trains are generated by NEST-native device named 'sinusoidal Poisson generator' with parameters in Table 1. Third, A1 Pyr cells project outputs to downstream neurons. These synaptic connections approximate the cortico-cortical projection from A1 to higher order auditory/cognitive areas, as superficial layers project directly to the higher order areas (Felleman & Van Essen, 1991; Markov & Kennedy, 2013). For simplicity, we did not consider any recurrent connection in the three external populations.

Neuron models

All three inhibitory cell types are implemented by neuron models proposed by Hill and Tononi (Hill & Tononi, 2005). The 'HT' neuron is a point neuron with simplified Hodgkin–Huxley currents. For reference, we provide a brief review of the neuron model; see (Hill & Tononi, 2005) for details.

The neuronal dynamics obey Equation 1:

$$\frac{dV}{dt} = \frac{[-g_{Na}(V-E_{Na})-g_{KL}(V-E_K)-I_{syn}-I_{int}]}{\tau_m} - g_{spike}(V-E_k)/\tau_{spike}. \quad (1)$$

Membrane potentials (V), decayed exponentially with time scale τ_m, are regulated by sodium (Na) and potassium (K) leak currents with conductance (g_{Na} and g_{KL}) and reversal potentials (E_{Na} and E_K). The fast hyperpolarization current during spikes is simulated with a rectangular spike with a conductance (g_{spike}) and decaying time constant (t_{spike}). Synaptic events induce dual exponential responses (I_{syn}) in the target neurons, which are described by rising (τ_1) and decaying time (τ_2) constants (Table 2). The reversal potentials for GABA and AMPA are -80 and 0 mV in the model. We did not consider NMDA synapses in the model. The intrinsic ion currents (Iint) are from the original model (Hill & Tononi, 2005).

Also, spike threshold (θ) evolves over time with equilibrium (θ_{eq}) and time constant (t_θ), as shown in Equation 2.

$$\frac{d\theta}{dt} = -(\theta-\theta_{eq})/\tau_\theta \quad (2)$$

The three cell types have different parameters listed in Table 3. We assume that cholinergic modulation innervates non-FS cells for experimental observations. First, basal forebrain, which provides cholinergic modulation to cortices (Sarter, Parikh, & Howe, 2009), mainly targets somatostatin positive (SST) interneurons (Chen, Sugihara, & Sur, 2015). Second, cholinergic modulation does not modulate the excitability of FS cells (Gulledge et al., 2007). Third, acetylcholine innervates low-threshold spiking interneurons known to express SST via nicotinic receptors but does not modulate the excitability of FS cells (Xiang et al., 1998).

Synaptic connections

All synapses in the model have static synaptic weights unlike the depressing synapses in the original model (Hill & Tononi, 2005). FS and non-FS cells provide fast and slowly decaying GABA connections on target neurons, respectively (Traub et al., 2005); 7 msec and 20 msec are chosen for decay time constants for fast and slow kinetics (Table 2). According to the observed pattern (Pfeffer, Xue, He, Huang, & Scanziani, 2013), non-FS cells corresponding to SST cells inhibit FS and Pyr cells, whereas FS cells inhibit FS cells and Pyr cells. These two inhibitory cell types are also consistent with the two functional groups (major regulator and inhibitory selective interneurons) from a recent survey (Jiang et al., 2015). Figure 1A shows the schematic of synaptic connections. When we connect pre-synaptic and post-synaptic populations, we connect cell pairs randomly using the connection probabilities (Table 4).

Simulation of local field potentials

We approximated EEG by calculating local field potentials (LFPs). LFPs were simulated by summing up all the synaptic currents in downstream neurons (Mazzoni, Panzeri, Logothetis, & Brunel, 2008). Then the spectral power density of LFPs was calculated via ‘scipy’ included in python. For each simulation condition, we ran 100 simulations, in which a network is independently instantiated using the same connectivity rule, and report the average LFP power from them.

Spike-triggered average of LFPs

The coherence between top-down gamma rhythms to A1 and synaptic inputs to downstream neurons was measured with spike-triggered average (STA) of LFPs. In each simulation, we aggregated the 100 msec LFP segments aligned to the spike times of HC cell population which projects top-down gamma rhythms into A1, and averaged them to calculate STA of LFPs. The

spectral power of STA of LFPs is calculated in each simulation, and we report the averaged power from 100 independent simulations.

Results

In this study, we simulated gamma rhythms reported in an experimental study (Spencer, 2011) by utilizing a network model (Figure 1A). That is, we used 40 Hz auditory click trains as stimuli in the stimulus period. As synaptic currents onto Pyr cells are the dominant factor for both LFPs and EEG (Destexhe & BEdard, 2013), we approximate EEG using LFPs calculated from the network model (Methods). The three cell types, implemented with HT neurons (Hill & Tononi, 2005), exhibit disparate responses to 20 pA tonic currents (Figure 1B); see Methods for details on neuron models. The most active cells are FS cells, and non-FS cells show frequency adaptation, which is consistent with experimental observation (Gibson, Beierlein, & Connors, 1999; Kawaguchi & Kubota, 1997). They are connected with cell type specific connectivity (Pfeffer et al., 2013).

HC and SC cells generate sinusoidal Poisson spike trains (Methods) independently and project them onto A1. HC cells generate 45 Hz top-down gamma rhythms mimicking top-down signals from an association cortex to A1 (Roopun et al., 2010). SC cells project 40 Hz gamma rhythms mimicking synaptic inputs into A1 induced by auditory click trains. According to experimental data (Couey et al., 2007a; Gulledge et al., 2007; Xiang et al., 1998), we assumed that cholinergic modulation depolarizes non-FS cells and reduced the excitability to simulate the disrupted cholinergic modulation in A1. Specifically, non-FS cells receive 100 Hz Poisson spike trains in the control condition, whereas those external inputs are removed in the pathological conditions (Table 3).

Reduced excitability of non-FS cells modulates gamma rhythms generated by A1 in the pre-stimulus and stimulus periods

In the first set of simulations, HC cells project 45 Hz gamma rhythms onto A1 during the entire duration (1 second), whereas SC cells project gamma rhythms for the last 500 msec. The first 500 msec simulation results are used to calculate the baseline gamma rhythms, while the last 500 msec simulation results are used to calculate the stimulus-evoked gamma rhythms. Figure 2A and B show the spikes of three cell types during simulations in the control and pathological conditions, respectively. Non-FS cells fire asynchronously in the control condition (Figure 2A), but they are quiescent in the pathological condition. FS cell activity appears to be stronger when non-FS cells are quiescent, whereas Pyr cell activity looks positively correlated with non-FS cell activity. We estimated LFPs in the downstream neurons, which reflect A1 outputs, in the pre-stimulus and stimulus periods, respectively. In the pre-stimulus period, 45 Hz rhythms are induced, and the baseline power strengthens in the pathological condition (Figure 2C). In the stimulus period, 45 Hz rhythms are reduced, and 40 Hz rhythms, consistent with bottom-up gamma rhythms, are generated (Figure 2D), suggesting that A1 responds to bottom-up gamma rhythms rather than top-down gamma rhythms. We note that A1 responses to the bottom-up gamma rhythms are higher in the control condition.

What roles do non-FS cells play in modulating A1 outputs?

The results above suggest that the reduced non-FS cells' excitability causes abnormal gamma rhythms in both pre-stimulus and stimulus periods. Then, what functions do non-FS cells perform in sensory signal processing? To better understand their functional roles, we ran simulations with varying inhibition strengths from non-FS cells to FS cells and from non-FS cells to Pyr cells. Figure 3 shows the spectral power of LFPs depending on the strengths of inhibition of non-FS

cells. The strength of inhibition onto Pyr cells is negatively correlated to the LFP power in the pre-stimulus period (Figure 3A). In contrast, the strength of inhibition onto FS cells is positively correlated with LFP power in the stimulus period (Figure 3B). These results suggest 1) that non-FS cells prevent A1 Pyr cells from responding to top-down gamma rhythms and 2) that they enhance the sensitivity of A1 Pyr cells to bottom-up gamma rhythms. As bottom-up inputs are introduced in the stimulus period only, we propose that non-FS cells ensure Pyr cells to fire strongly only when the bottom-up signals are present.

Top-down gamma rhythms can subserve corollary discharge

To study the potential functions of top-down gamma rhythms, we estimated the effects of top-down gamma rhythms on Pyr cells' spontaneous activity. In this experiment condition, Pyr cells are driven purely by external background inputs (Table 3), and the top-down gamma rhythms are projected onto A1 between 200-1000 msec during 2200 msec-long simulations. Figure 4A shows an example from our simulation results. During the top-down gamma rhythm projection (200-1000 msec), FS cell activity is enhanced, but Pyr cell activity is reduced, indicating that top-down gamma rhythms suppress Pyr cell activity by innervating FS cells. To test this assertion further, we examine the effects of top-down gamma rhythms as a function of the amplitudes of top-down gamma rhythms (Methods). Figure 4B shows how effectively top-down gamma rhythms suppress Pyr cell activity. R in the y-axis is the average firing rate of Pyr cells between 200-1000 msec divided by those between 1200-2000 msec when no top-down gamma rhythms are projected. The mean values of R from 100 simulations decrease, as the amplitude of top-down gamma rhythms, generated by HC cells, increase. This suggests that gamma rhythms are suppressive of Pyr cell activity.

If top-down signals suppress A1 responses, they may subserve corollary discharge which suppresses auditory cortex when the self-generated sound is present. Also a line of studies suggests that auditory hallucination is induced by faulty corollary discharge (Blakemore, Smith, Steel, Johnstone, & Frith, 2000; Ford & Mathalon, 2005). Thus, we hypothesize that disrupted cholinergic modulation in A1 can underlie auditory hallucination. To address this possibility, we estimated the spike-triggered average of LFPs (see Methods) using HC cells' spikes. The peak of spectral power of STA of LFPs is at 45 Hz (Figure 4C), suggesting that top-down gamma rhythms impinging onto A1 can induce synaptic inputs in the downstream neurons. More importantly, LFP power reflecting this erroneous activation of A1 Pyr cells is stronger in the pathological condition, supporting that cholinergic modulation can cause auditory hallucination.

Discussion

Our simulation results support the potential links between disrupted cholinergic modulation and enhanced gamma rhythms in the baseline period. Non-FS cells in the model prevent Pyr cells' erroneous activation in the pre-stimulus period and increase their responses to sensory stimuli in the stimulus period. That is, when non-FS cells cannot perform those functions, the interareal interactions involving A1 would be aberrant, shedding light on the potential pathophysiology underlying 'functional' dysconnectivity. As acetylcholine is known to depolarize non-FS cells via nicotinic receptors (Couey et al., 2007a; Xiang et al., 1998), the symptoms induced by disrupted cholinergic modulation can be alleviated by enhancing the concentration of nicotine. This could explain the precognitive effects of smoking (Sacco, Bannon, & George, 2004).

Below we discuss the implications of our simulation results in more details.

Implications for positive symptoms

A1 responses are suppressed by corollary discharge (Nelson et al., 2013; Schneider, Nelson, & Moony, 2014), and thus they would be abnormally strong when the corollary discharge is disturbed. In the model, disrupted cholinergic modulation leads to the stronger erroneous activation of A1 in response to top-down gamma rhythms (Figure 4C). This result supports the hypothetical link between corollary discharge and auditory hallucination (Blakemore et al., 2000; Ford & Mathalon, 2005) and further suggests that auditory hallucination can reflect the content of top-down signals. More specifically, if top-down signals subserving corollary discharge mediate inner speech (Cho & Wu, 2013), A1 could turn this imaginary information into real sensory signals in the pathological condition; A1 is indeed hyperactive during hallucination (Dierks et al., 1999; L., M., P., & E., 2002). This can explain potential mechanisms by which aberrant corollary discharge induces auditory hallucination in human voice. Interestingly, abnormal baseline gamma rhythms have been found stronger in the left-hemisphere (Spencer, 2011), which is associated with language processing.

Implications for negative symptoms

A1 responses to sensory stimuli are reduced in the pathological condition, impacting auditory perception directly. Could it be related to negative symptoms of schizophrenia? A precise correlation between A1 responses and negative symptoms of schizophrenia may prove difficult to find, but the reduction of A1 responses could impair some developmental processes. If the primary sensory responses are weaker than the normal ones, the developing mechanisms relying on the external stimuli could be impaired. In this way, the reduced A1 responses may contribute to the schizophrenia's negative symptoms.

The limits of the model and future direction

It should be noted that we ignore the potential contribution of N-methyl-D-aspartate (NMDA) receptor hypofunction despite the well-known observation that the pathology of schizophrenia involves NMDA receptor hypofunction (Jadi, Margarita Behrens, & Sejnowski, 2015; Pittman-Polletta et al., 2015). This exclusion is due to the lack of information on the functional roles of NMDA synapses and their complex modulation of gamma rhythms (Hunt & Kasicki, 2013; Kirli, Ermentrout, & Cho, 2014). As NMDA antagonist increases gamma rhythms in cingulate areas (Wood, Kim, & Moghaddam, 2012), we plan to extend our model to incorporate higher cognitive areas and investigate the coordination between NMDA receptors and cholinergic gating in the auditory perception, with which we could explore more implications for schizophrenia's pathology.

Acknowledgments

We wish to thank the Allen Institute founders, Paul G. Allen and Jody Allen, for their vision, encouragement and support.

Financial Disclosures

Dr. Lee is an employee at Allen Institute for Brain Science, a non-profit research organization, and has not received any other financial support.

References

Andreou, C., Nolte, G., Leicht, G., Polomac, N., Hanganu-Opatz, I. L., Lambert, M., … Mulert, C. (2015). Increased Resting-State Gamma-Band Connectivity in First-Episode Schizophrenia. *Schizophrenia Bulletin*, *41*(4), 930–939.

http://doi.org/10.1093/schbul/sbu121

Blakemore, S. J., Smith, J., Steel, R., Johnstone, C. E., & Frith, C. D. (2000). The perception of self-produced sensory stimuli in patients with auditory hallucinations and passivity experiences: evidence for a breakdown in self-monitoring. *Psychological Medicine*, *30*(5), 1131–9. http://doi.org/10.1017/S0033291799002676

Chen, N., Sugihara, H., & Sur, M. (2015). An acetylcholine-activated microcircuit drives temporal dynamics of cortical activity. *Nature Neuroscience*, *18*(6), 892–902. http://doi.org/10.1038/nn.4002

Cho, R., & Wu, W. (2013). Mechanisms of auditory verbal hallucination in schizophrenia. *Frontiers in Psychiatry*, *4*(NOV), 1–8. http://doi.org/10.3389/fpsyt.2013.00155

Couey, J. J., Meredith, R. M., Spijker, S., Poorthuis, R. B., Smit, A. B., Brussaard, A. B., & Mansvelder, H. D. (2007a). Distributed Network Actions by Nicotine Increase the Threshold for Spike-Timing-Dependent Plasticity in Prefrontal Cortex. *Neuron*, *54*, 73–87. http://doi.org/10.1016/j.neuron.2007.03.006

Couey, J. J., Meredith, R. M., Spijker, S., Poorthuis, R. B., Smit, A. B., Brussaard, A. B., & Mansvelder, H. D. (2007b). Distributed network actions by nicotine increase the threshold for spike-timing-dependent plasticity in prefrontal cortex. *Neuron*, *54*(1), 73–87. http://doi.org/10.1016/j.neuron.2007.03.006

Damaraju, E., Allen, E. A., Belger, A., Ford, J. M., McEwen, S., Mathalon, D. H., … Calhoun, V. D. (2014). Dynamic functional connectivity analysis reveals transient states of dysconnectivity in schizophrenia. *NeuroImage: Clinical*, *5*(July), 298–308.

http://doi.org/10.1016/j.nicl.2014.07.003

Destexhe, A., & BEdard, C. (2013). Local field potential. *Scholarpedia*, *8*(8), 10183.

Dierks, T., Linden, D. E., Jandl, M., Formisano, E., Goebel, R., Lanfermann, H., & Singer, W. (1999). Activation of Heschl's gyrus during auditory hallucinations. *Neuron*, *22*(3), 615–621. http://doi.org/10.1016/S0896-6273(00)80715-1

Felleman, D. J., & Van Essen, D. C. (1991). Distributed hierarchical processing in the primate cerebral cortex. *Cerebral Cortex (New York, N.Y. : 1991)*, *1*(1), 1–47. Retrieved from http://www.ncbi.nlm.nih.gov/pubmed/1822724

Flynn, G., Alexander, D., Harris, A., Whitford, T., Wong, W., Galletly, C., … Williams, L. M. (2008). Increased absolute magnitude of gamma synchrony in first-episode psychosis. *Schizophrenia Research*, *105*(1-3), 262–71. http://doi.org/10.1016/j.schres.2008.05.029

Ford, J. M., & Mathalon, D. H. (2005). Corollary discharge dysfunction in schizophrenia: Can it explain auditory hallucinations? *International Journal of Psychophysiology*, *58*(2-3 SPEC. ISS.), 179–189. http://doi.org/10.1016/j.ijpsycho.2005.01.014

Fries, P. (2005). A mechanism for cognitive dynamics: neuronal communication through neuronal coherence. *Trends in Cognitive Sciences*, *9*(10), 474–80. http://doi.org/10.1016/j.tics.2005.08.011

Gewaltig, M.-O., & Diesmann, M. (2007). NEST (NEural Simulation Tool). *Scholarpedia*, *2*(4), 1430.

Gibson, J. R., Beierlein, M., & Connors, B. W. (1999). Two networks of electrically coupled inhibitory neurons in neocortex. *Nature*, *402*(6757), 75–9. http://doi.org/10.1038/47035

Goñi, J., van den Heuvel, M. P., Avena-Koenigsberger, A., Velez de Mendizabal, N., Betzel, R. F., Griffa, A., … Sporns, O. (2014). Resting-brain functional connectivity predicted by analytic measures of network communication. *Proceedings of the National Academy of Sciences of the United States of America*, *111*(2), 833–8. http://doi.org/10.1073/pnas.1315529111

Gregoriou, G. G., Gottes, S. J., Zhou, H., & Desimone, R. (2008). visual cortex during attention. *Science*, *324*(5931), 1207–1210. http://doi.org/10.1126/science.1171402.

Gulledge, A. T., Park, S. B., Kawaguchi, Y., & Stuart, G. J. (2007). Heterogeneity of Phasic Cholinergic Signaling in Neocortical Neurons, 2215–2229. http://doi.org/10.1152/jn.00493.2006.

Hill, S., & Tononi, G. (2005). Modeling Sleep and Wakefulness in the Thalamocortical System. *Journal of Neurophysiology*, *93*(3), 1671–1698. http://doi.org/10.1152/jn.00915.2004

Hunt, M. J., & Kasicki, S. (2013). A systematic review of the effects of NMDA receptor antagonists on oscillatory activity recorded in vivo. *Journal of Psychopharmacology (Oxford, England)*, *27*(11), 972–86. http://doi.org/10.1177/0269881113495117

Jadi, M. P., Margarita Behrens, M., & Sejnowski, T. J. (2015). Abnormal Gamma Oscillations in N-Methyl-D-Aspartate Receptor Hypofunction Models of Schizophrenia. *Biological Psychiatry*, *79*(9), 716–726. http://doi.org/10.1016/j.biopsych.2015.07.005

Jiang, X., Shen, S., Cadwelll, C., Berence, P., Sinz, F., Ecker, A. S., … Tolias, A. S. (2015). Principles of connectivity among morphologically defined cell types in adult neocortex. *Science*, *350*(6264).

Kawaguchi, Y., & Kubota, Y. (1997). GABAergic cell subtypes and their synaptic connections in rat frontal cortex. *Cerebral Cortex (New York, N.Y. : 1991)*, *7*(6), 476–86. Retrieved from http://www.ncbi.nlm.nih.gov/pubmed/9276173

Kirli, K. K., Ermentrout, G. B., & Cho, R. Y. (2014). Computational study of NMDA conductance and cortical oscillations in schizophrenia. *Frontiers in Computational Neuroscience*, *8*(October), 133. http://doi.org/10.3389/fncom.2014.00133

Kwon, J. S., O'Donnell, B. F., Wallenstein, G. V., Greene, R. W., Hirayasu, Y., Nestor, P. G., … McCarley, R. W. (1999). Gamma Frequency–Range Abnormalities to Auditory Stimulation in Schizophrenia. *Archives of General Psychiatry*, *56*(11), 1001. http://doi.org/10.1001/archpsyc.56.11.1001

L., A. B., M., B., P., L., & E., S. (2002). Cerebral activity associated with auditory verbal hallucinations: A functional magnetic resonance imaging case study. *Journal of Psychiatry and Neuroscience*, *27*(2), 110–115. Retrieved from http://www.embase.com/search/results?subaction=viewrecord&from=export&id=L34478362\nhttp://sfx.library.uu.nl/utrecht?sid=EMBASE&issn=11804882&id=doi:&atitle=Cerebral+activity+associated+with+auditory+verbal+hallucinations:+A+functional+magnetic+resonance

Lee, J. H., Whittington, M. A., & Kopell, N. J. (2015). Potential Mechanisms Underlying Intercortical Signal Regulation via Cholinergic Neuromodulators. *Journal of Neuroscience*, *35*(45), 15000–15014. http://doi.org/10.1523/JNEUROSCI.0629-15.2015

Markov, N. T., & Kennedy, H. (2013). The importance of being hierarchical. *Current Opinion in Neurobiology*, *23*(2), 187–94. http://doi.org/10.1016/j.conb.2012.12.008

Mazzoni, A., Panzeri, S., Logothetis, N. K., & Brunel, N. (2008). Encoding of naturalistic stimuli by local field potential spectra in networks of excitatory and inhibitory neurons. *PLoS Computational Biology*, *4*(12), e1000239. http://doi.org/10.1371/journal.pcbi.1000239

Nelson, A., Schneider, D. M., Takatoh, J., Sakurai, K., Wang, F., & Mooney, R. (2013). A circuit for motor cortical modulation of auditory cortical activity. *The Journal of Neuroscience : The Official Journal of the Society for Neuroscience*, *33*(36), 14342–53. http://doi.org/10.1523/JNEUROSCI.2275-13.2013

Pettersson-Yeo, W., Allen, P., Benetti, S., McGuire, P., & Mechelli, A. (2011). Dysconnectivity in schizophrenia: Where are we now? *Neuroscience and Biobehavioral Reviews*, *35*(5), 1110–1124. http://doi.org/10.1016/j.neubiorev.2010.11.004

Pfeffer, C. K., Xue, M., He, M., Huang, Z. J., & Scanziani, M. (2013). Inhibition of inhibition in visual cortex: the logic of connections between molecularly distinct interneurons. *Nature Neuroscience*, *16*(8), 1068–76. http://doi.org/10.1038/nn.3446

Pittman-Polletta, B. R., Kocsis, B., Vijayan, S., Whittington, M. A., & Kopell, N. J. (2015). Brain rhythms connect impaired inhibition to altered cognition in schizophrenia. *Biological Psychiatry*, *77*(12), 1020–1030. http://doi.org/10.1016/j.biopsych.2015.02.005

Roopun, A. K., Lebeau, F. E. N., Ramell, J., Cunningham, M. O., Traub, R. D., & Whittington, M. a. (2010). Cholinergic neuromodulation controls directed temporal communication in neocortex in vitro. *Frontiers in Neural Circuits*, *4*(March), 8. http://doi.org/10.3389/fncir.2010.00008

Sacco, K. A., Bannon, K. L., & George, T. P. (2004). Nicotinc receptor mechanisms and

cognition in normal states and neuropsychiatric disorders. *J Psychopharmacol.*, *18*(4), 457–474.

Sarter, M., Parikh, V., & Howe, W. M. (2009). Phasic acetylcholine release and the volume transmission hypothesis: time to move on. *Nature Reviews. Neuroscience*, *10*(5), 383–90. http://doi.org/10.1038/nrn2635

Schneider, D., Nelson, A., & Moony, R. (2014). NA synaptic and circuit basis for corollary discharge in the auditory cortexo Title. *Nature*, *513*, 189–194.

Spencer, K. M. (2009). The functional consequences of cortical circuit abnormalities on gamma oscillations in schizophrenia: insights from computational modeling. *Frontiers in Human Neuroscience*, *3*(October), 33. http://doi.org/10.3389/neuro.09.033.2009

Spencer, K. M. (2011). Baseline gamma power during auditory steady-state stimulation in schizophrenia. *Frontiers in Human Neuroscience*, *5*(January), 190. http://doi.org/10.3389/fnhum.2011.00190

Traub, R. D., Contreras, D., Cunningham, M. O., Murray, H., LeBeau, F. E. N., Roopun, A., … Whittington, M. a. (2005). Single-column thalamocortical network model exhibiting gamma oscillations, sleep spindles, and epileptogenic bursts. *Journal of Neurophysiology*, *93*(4), 2194–232. http://doi.org/10.1152/jn.00983.2004

Uhlhaas, P. J. (2013). Dysconnectivity, large-scale networks and neuronal dynamics in schizophrenia. *Current Opinion in Neurobiology*, *23*(2), 283–290. http://doi.org/10.1016/j.conb.2012.11.004

Uhlhaas, P., & Singer, W. (2010). Abnormal neural oscillations and synchrony in schizophrenia.

Nature Reviews Neuroscience, *11*, 100–113.

van den Heuvel, M. P., & Hulshoff Pol, H. E. (2010). Exploring the brain network: A review on resting-state fMRI functional connectivity. *European Neuropsychopharmacology*, *20*(8), 519–534. http://doi.org/10.1016/j.euroneuro.2010.03.008

Vierling-Claassen, D., Cardin, J. a, Moore, C. I., & Jones, S. R. (2010). Computational modeling of distinct neocortical oscillations driven by cell-type selective optogenetic drive: separable resonant circuits controlled by low-threshold spiking and fast-spiking interneurons. *Frontiers in Human Neuroscience*, *4*(November), 198. http://doi.org/10.3389/fnhum.2010.00198

Vierling-Claassen, D., Siekmeier, P., Stufflebeam, S., & Kopell, N. (2008). Modeling GABA alterations in schizophrenia: a link between impaired inhibition and altered gamma and beta range auditory entrainment. *Journal of Neurophysiology*, *99*, 2656–2671. http://doi.org/10.1152/jn.00870.2007

Wood, J., Kim, Y., & Moghaddam, B. (2012). Disruption of Prefrontal Cortex Large Scale Neuronal Activity by Different Classes of Psychotomimetic Drugs. *The Journal of Neuroscience*, *32*(9), 3022–3031. http://doi.org/10.1523/JNEUROSCI.6377-11.2012

Xiang, Z., Huguenard, J. R., & Prince, D. A. (1998). Cholinergic Switching Within Neocortical Inhibitory Networks. *Science*, *281*(5379), 985–988. http://doi.org/10.1126/science.281.5379.985

Legends

Figure 1: The structure of the model. (A) The superficial layer of A1 is explicitly modeled using three cell types (Pyr, FS and non-FS cells in red, blue and green, respectively). In the model, there are three external populations (shown as ovals) of Pyr cells interacting with A1. The first two populations (HC and SC) project top-down and bottom-up gamma rhythms into A1, and each individual Pyr cell in the populations fires inhomogeneous Possion spikes rate of either 40 Hz or 45 Hz depending on the population. The last population (downstream neurons) receives synaptic inputs from A1 Pyr cells. (B) The firing patterns of the three cell types in response to 20 pA tonic current injection.

Figure 2: The network responses depending on the excitability of non-FS cells. (A) Red, blue and green dots represent action potentials of Pyr, non-FS and FS cells during a simulation. Each row in the y-axis is the ids of cells. The left and right columns compare spiking activity with and without non-FS cell firing. (B) The comparison between spectral powers in downstream neurons with and without non-FS cell firing. The left and right columns illustrate the pre-stimulus and stimulus periods, respectively.

Figure 3: The effects of inhibition of non-FS cells. (A) The modulation LFP power via inhibition from non-FS to FS cells in the pre-stimulus period. (B) The modulation of LFP power via inhibition from non-FS to Pyr cells in the stimulus period.

Figure 4: The functional roles of top-down gamma rhythms. (A) Spike activity with top-down gamma rhythms introduced between 200-1000 msec indicated by the black arrow. (B) The reduction of Pyr cell activity depending on amplitudes of top-down gamma rhythms. (C) The spectral power of STA of LFP using spikes of top-down gamma rhythms.

Table 1: Parameters for sinusoidal Poisson generator. This NEST-native device (Gewaltig & Diesmann, 2007) generates inhomogeneous oscillatory spike trains depending on the three parameters, 'amplitude (ac)', 'baseline (dc)' and 'frequency'. For HC and SC, we use the values shown below.

Table 2: Synaptic parameters. All synapses are static and induce double exponential responses described by τ_1 and τ_2. g_{peak} and E_{rev} are the conductance of the synapses and reversal potentials.

Table 3: Neuronal parameters. We list the parameters chosen for the three cell types. g_T is the conductance of low-threshold currents (Hill & Tononi, 2005), and the frequency of external background inputs to each cell type is shown in the last column. All cells are implemented using NEST-native neuron models named "ht_neurons" (Gewaltig & Diesmann, 2007), and non-specified parameters are the same as defaults values in NEST.

Table 4: Connectivity. Connections are randomly generated using the following connectivity. The weights are used to scale synaptic strength (Gewaltig & Diesmann, 2007).

Tables

Table 1

	Amplitude (Hz)	Baseline (Hz)	Frequency (Hz)
HC	60	0	45
SC	60	0	40

Table 2

	g_{peak}	τ_1	τ_2	E_{rev} (mV)
AMPA	0.1	0.5	2.4	0
GABA from FS	0.33	1.0	7.0	-80
GABA from non-FS	0.33	1.0	20.0	-80

Table 3

	NaP	t_{spike}	θ_{eq} (mV)	τ_m (msec)	τ_θ (msec)	g_T	Ext (Hz)
Pyr	1.0	2.0	-51	16.0	2.0	2.0	200
FS	1.0	2.0	-53	8.0	1.0	1.0	100
Non-FS	1.0	2.0	-53	8.0	1.0	2.0	100

Table 4

Connection type	Connection probability	Weights
External background	N/A	3.0
Pyr→Pyr	0.4	0.075
Pyr→FS	0.4	0.45
Pyr→non-FS	0.2	0.15
FS→FS	1.0	0.15
FS→Pyr	0.4	0.6
Non-FS→FS	0.4	0.6
Non-FS→Pyr	0.4	0.39
HC to Pyr	0.2	0.09
HC to FS	0.2	0.18
SC to Pyr	0.2	0.18
SC to FS	0.2	0.18
Pyr→downstream	0.2	0.15

Figures

Figure 1

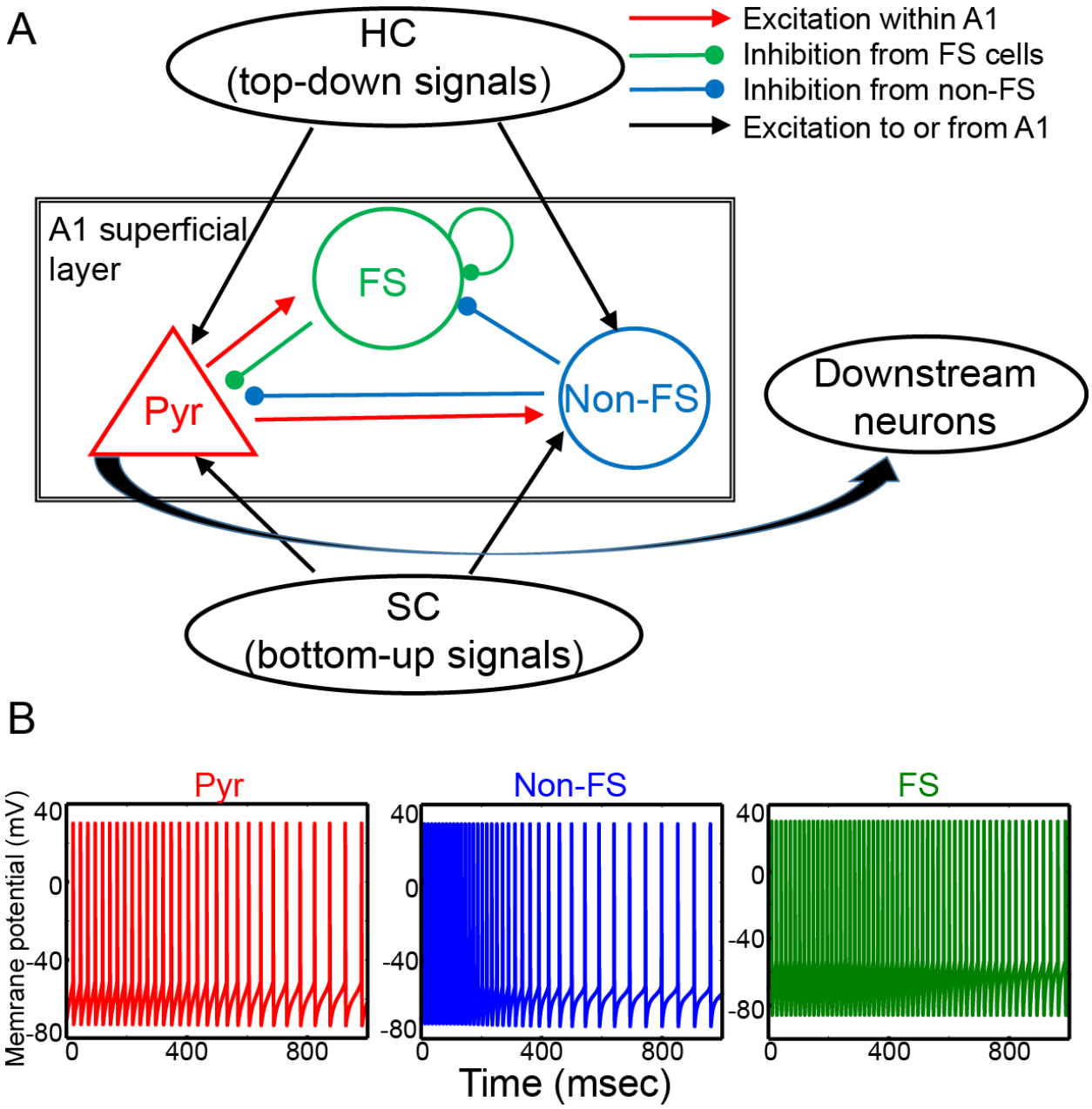

Figure 2

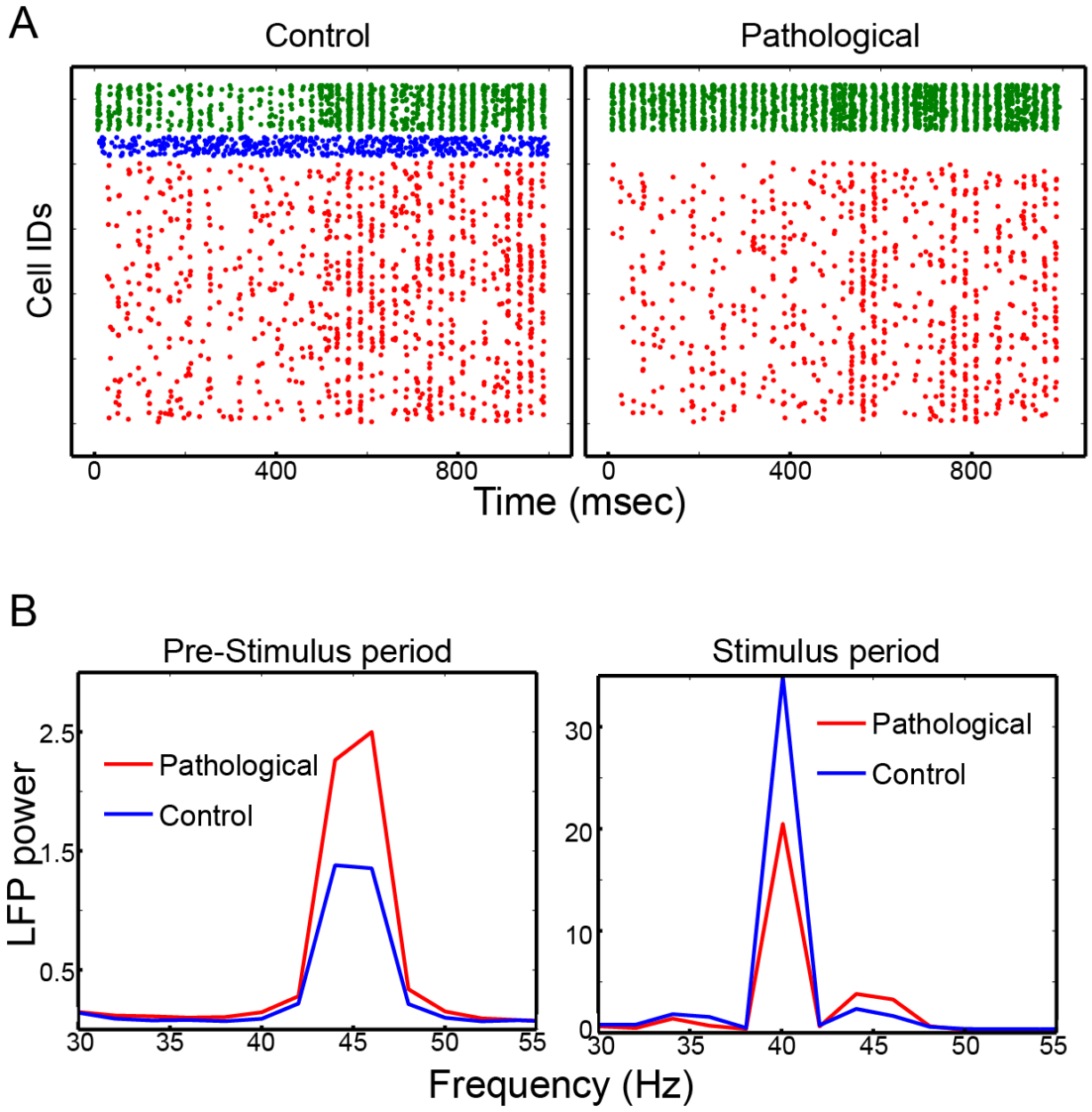

Figure 3

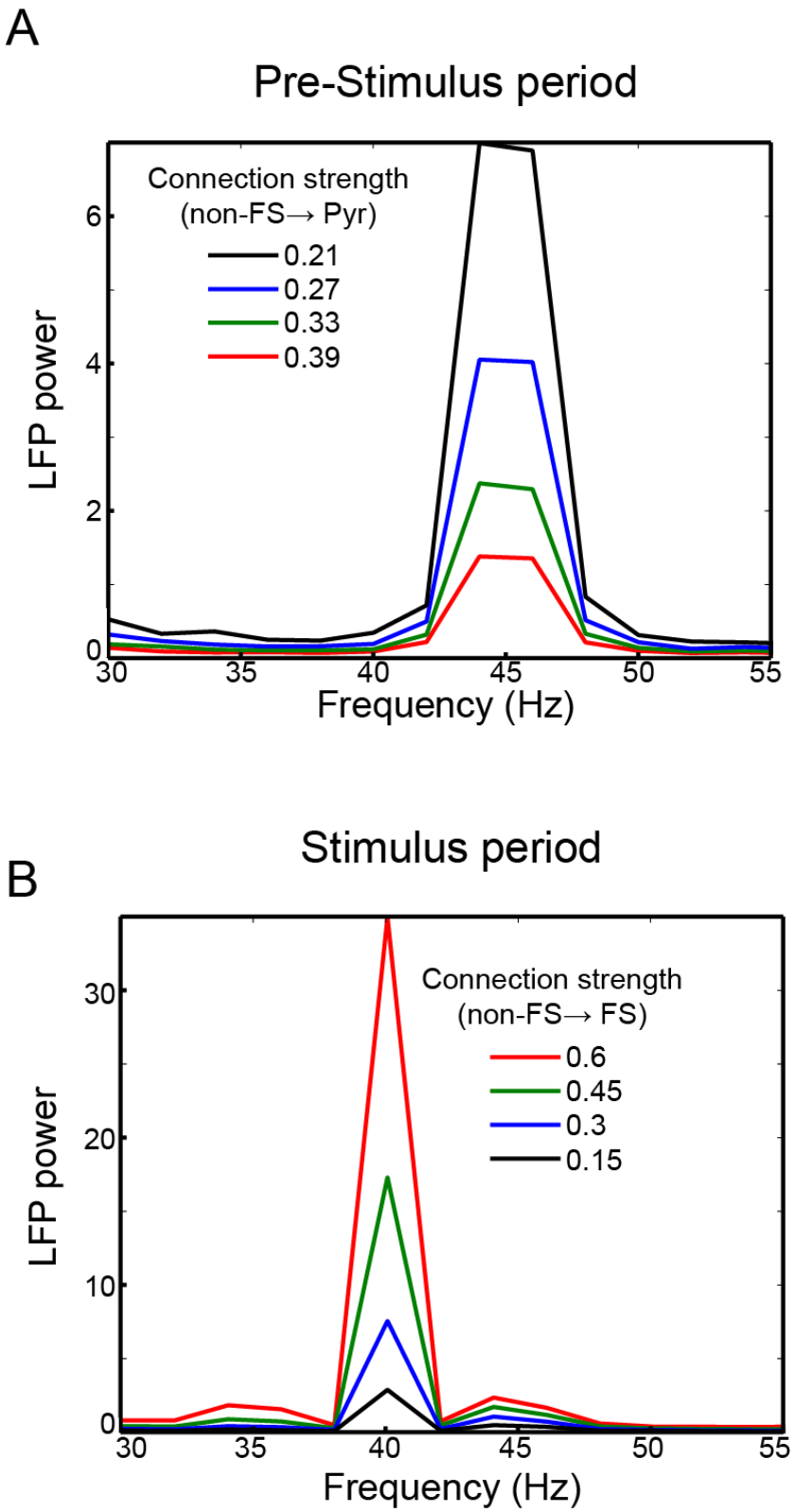

Figure 4